Coordinated Control of High-Order Fully Actuated Multiagent Systems and Its Application: A Predictive Control Strategy

Da-Wei Zhang, *Student Member, IEEE*, Guo-Ping Liu, *Fellow, IEEE*, and Lei Cao

***Abstract*—This research is devoted to the coordinated control of high-order fully actuated multiagent systems (HOFA-MASs). A predictive control strategy is developed to realize the coordination of HOFA-MASs and simultaneous stability and output consensus. In this strategy, a Diophantine equation is introduced to construct an incremental HOFA prediction model rather than a reduced-order one, then a cost function focused on coordinated relationship is minimized by the design of predictive control such that the optimal coordination controllers can be achieved with simple and easy computation. Further discussion derives a simple criterion to guarantee the simultaneous stability and output consensus of the closed-loop HOFA-MASs. Two experiments of formation control of three air-bearing simulators are given to demonstrate the availability of the predictive control strategy.**

***Index Terms*—Coordinated control, formation control of air-bearing simulators, high-order fully actuated (HOFA) multiagent systems (MASs) (HOFA-MASs), predictive control, simultaneous stability and output consensus.**

I. Introduction

At the concept of Internet of Things has been deeply rooted among the people, the multiagent system (MAS) has become one of the hottest research fields and has been widely applied in smart grid [1], multiple UAV systems [2], distribution systems [3], microgrid [4], and other applications (see [5]–[7]). In this issue, coordinated control considers the realization of global and individual aims based on a networked control protocol, which has attracted great interests of scholars and has obtained a string of achievements.

Recently, Li *et al.* [8] presented a new consensus control protocol to design a dynamic compensator with strict state tracking, such that the time delays can be compensated. Tan *et al.* [9] proposed a novel distributed protocol according to Lyapunov theories and the stochastic analysis method to cope with the consensus problem of leader–follower stochastic MASs. Wang *et al.* [10] gave a disturbance observer to estimate the exact states with local disturbances so that the fully leaderless consensus control problem is dealt with. Tan *et al.* [11] aimed at communication constraints to consider a data-driven distributed control based on cloud computing, a highlight of this scheme is that it is independent on the system model. Cheng and Li[12] designed an event-triggered protocol based on a static asynchronous edge and an adaptive one, respectively, to solve the difficulties of network heterogeneous caused by leader with unknown input such that the leader–follower consensus is achieved. Mehdifar *et al.* [13] discussed a robust formation control protocol to cope with unknown disturbances, the presented results are illustrated based on Lyapunov and graph theories. In [14], a two-layer control structure is established via mixed graph theory and optimal control, such that two robust gains are obtained to ensure the exponential stability of two-layer interconnected MAS. In [15], the distributed consensus of MASs is achieved by a Zeno-free self-triggered method, an obvious advantage in that is to lead into a positive $\mathcal{L}^p$ signal of event-detected function such that triggered events can be effectively reduced within a finite-time interval. In [16], a bounded consensus criteria is established to ensure the coordinated tracking subject to bounded intermittent communication and dynamical interaction topology. In addition, the works in [17]–[20] and other relative achievements also have contributions to the development of this research field. Among so many methods, predictive control can effectively cope with some constraints in coordinated control, such as communication delays, packet dropouts, and cyber attacks, and can be easily implemented in practice with great efficiency, flexibility, and other benefits, such that many researchers pay closed attention to it. Liu[21], [22] proposed a networked predictive control strategy to compensate the network constraints and implement the coordination of MASs for linear and data-driven cases. Pang *et al.* [23] proposed an incremental predictive control scheme to deal with the random delays and packet dropouts during the

Manuscript received 9 December 2021; revised 21 January 2022; accepted 28 February 2022. Date of publication 18 March 2022; date of current version 14 December 2022. Recommended by Technical Editor A. Alanis and Senior Editor M. Basin. This work was supported in part by the National Natural Science Foundation of China under Grant 62173255 and Grant 62188101. *(Corresponding author: Guo-Ping Liu.)*

Da-Wei Zhang and Lei Cao are with the Center for Control Theory and Guidance Technology, Harbin Institute of Technology, Harbin 150001, China (e-mail: 20B904021@stu.hit.edu.cn; 18b904027@stu.hit.edu.cn).

Guo-Ping Liu is with the Center for Control Theory and Guidance Technology, Harbin Institute of Technology, Harbin 150001, China, and also with the Department of Electronic and Electrical Engineering, Southern University of Science and Technology, Shenzhen 518055, China (e-mail: liugp@sustech.edu.cn).

Color versions of one or more figures in this article are available at https://doi.org/10.1109/TMECH.2022.3156587.

Digital Object Identifier 10.1109/TMECH.2022.3156587

cooperative control of MASs. In [24], a cloud predictive control is presented to handle the DoS attacks, so that the attack-induced packet dropouts are compensated actively and the consensus condition is derived. There are also other results on predictive control based coordinated control for MASs (see [25]–[27] and the references therein).

However, a shortcoming in the abovementioned is that most of them still use first-order state-space (FOSS) model to describe the dynamical model of MAS, which results in the lost of physical meanings of original systems and ill-conditioned matrices in model reduction. Actually, second- and high-order systems are natural representation of physical systems, because their dynamical models, described by Newton's laws, Euler and Lagrangian equations, and so on, are in fact second and high order differential equations, which has been succeeded in the modeling and control of spacecrafts rendezvous [28], chaotic systems synchronization [29], and so on.

Inspired by [30], the high-order fully actuated (HOFA) system has been generalized as a general model of control systems, because it physically exists in the real-world and also can be converted from other underactuated systems, such as strict feedback systems, interconnected systems, and affine systems (see [31]). Compared to the FOSS model, one of the improvements of the HOFA system is that it is directly established by physical laws without model reduction. Not only is it a more natural representation of actual systems, it also maintains some important properties, which is used for the analysis and control of systems (see [32]). The other is that the HOFA system is a model oriented for control design, it is convenient to perfect the complete expression of control law. Obviously, the HOFA model for MASs may lead a novel and interesting topic on the analysis and control of MASs and associated studies, while there is still a blank. Coordinated control of MASs subject to communication delays, random disturbances, cyber attacks, game theories, group coordination, and other related problems will be reconstructed and resolved via HOFA model, which we are working toward. In this article, a basic problem of coordinated control for HOFA-MASs is discussed as a foundation for our later complicated studies. For this issue, one of the key problems is to design a coordinated control protocol based on the HOFA model rather than a reduced-order model with simple computation and powerful function, another is how to ensure the simultaneous stability and output consensus of the closed-loop HOFA-MASs under the presented control protocol.

For HOFA-MASs, this study aims to develop a predictive control strategy to realize the coordination performance. The major work is summarized as two aspects. On the one hand, a predictive control strategy is presented to achieve the coordination of HOFA-MASs. This strategy consists of local feedback control and networked predictive control. A local feedback is applied to maintain the closed-loop nominal HOFA-MAS (CNHOFA-MAS) is stable, which provides a better foundation for the coordination. Then, a Diophantine equation is used to establish an incremental HOFA prediction model instead of a reduced-order one, further a cost function considered coordinated relationship can be minimized by multistep output predictions, so that the complete optimal coordination controllers are constructed. On the other hand, a simple condition is provided to guarantee the simultaneous stability and output consensus of the closed-loop HOFA-MASs. This criterion is easy to verify and generalize to practical applications, which perfects the coordinated control based on predictive control in theory and practice. Moreover, two experiments of formation control of three air-bearing simulators are carried out, the experimental results show the desired formation can be implemented by the proposed control strategy, such that the availability of the predictive control strategy is further demonstrated. The highlights of this article are summarized as follows:

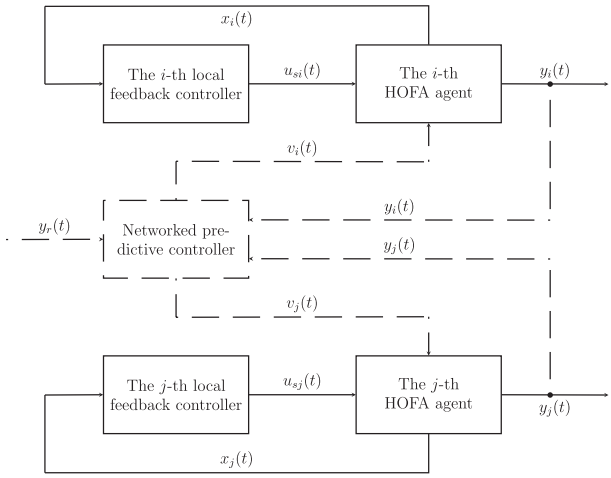

Fig. 1. Coordinated control of HOFA-MASs.

1) The HOFA model is introduced to describe the dynamical behaviors of MASs, which maintains the physical meanings of original systems and is also easy to complete the expression of control law.
2) A Diophantine equation is proposed to establish an incremental HOFA prediction model. Meanwhile, it is based on a closed-loop system rather than an open-loop one so that coordination performance can be implemented conveniently.
3) The design of both local feedback and networked predictive control are based on the HOFA model, which guarantees the HOFA features and practical meanings of controller coefficients and avoids the ill-conditioned matrices and other shortcomings in model reduction.

Compared to [33] and [34], the advantages are concluded in two aspects. On the one hand, this study investigates the truly high-order MASs, that is, the state variable is regarded as a n_i-dimension vector, and also be considered its nth difference equation. On the other hand, this study realizes the coordination by optimizing a cost function associated with coordinated relationship, which results in a more better dynamical performance.

II. Problem Formulation

The coordinated control of HOFA-MASs is shown in Fig. 1, whose interaction is considered by a directed graph $\mathcal{G} = \{\mathcal{N}, \mathcal{E}, \mathcal{A}\}$, where $\mathcal{N} = \{1, 2, \ldots, N\}$ and $\mathcal{E} \subset \mathcal{N} \times \mathcal{N}$ represent the set and edge set of HOFA-MASs, $\mathcal{A} = \{a_{ij}\}$ is an

adjacent matrix with $a_{ij} \geqq 0$ and $a_{ii} = 0$, $(i,j) \in \mathcal{E}$ denotes the ith HOFA-MAS communicates with the jth one via network in terms of associated adjacent element a_{ij}, $\mathcal{N}_i = \{j | j \in \mathcal{N}, j \neq i\}$. Then, the mathematical model of the ith HOFA-MAS is given as follows:

$$x_i(t+n) + \sum_{j=0}^{n-1} A_{ij} x_i(t+j) = B_i u_i(t), y_i(t) = C_i x_i(t) \tag{1}$$

where $i \in \mathcal{N}$, x_i, $u_i \in \mathbb{R}^{n_i}$, $y_i \in \mathbb{R}^m$ denote the state vector, control input, and actual output, $A_{ij} \in \mathbb{R}^{n_i \times n_i}$, $j = 0, 1, \ldots, n-1$, $B_i \in \mathbb{R}^{n_i \times n_i}$, $C_i \in \mathbb{R}^{m \times n_i}$ are given coefficients, and $\det(B_i) \neq 0$. There are some assumptions for HOFA-MAS (1).

Assumption 1:

A1 All state variables of HOFA-MAS (1) are available.

A2 The topology $\mathcal{G}$ is fixed and adjacent matrix $\mathcal{A}$ is constant.

A3 All clocks are synchronized and data transmitted are with time stamps.

For HOFA-MAS (1), a predictive control strategy is presented as

$$u_i(t) = B_i^{-1}(u_{si}(t) + v_i(t)), u_{si}(t) = \sum_{j=0}^{n-1} K_{ij} x_i(t+j) \tag{2}$$

where $K_{ij} \in \mathbb{R}^{n_i \times n_i}$, $j = 0, 1, \ldots, n-1$, are feedback coefficients to be solved, $v_i(t) \in \mathbb{R}^{n_i}$ is the prediction part, and B_i^{-1} is a known feedback gain to cope with the input coupling of controller, which is easy for the physical implementation. With predictive control strategy (2), the closed-loop HOFA-MAS is realized as

$$x_i(t+n) + \sum_{j=0}^{n-1} A_{ijc} x_i(t+j) = v_i(t) \tag{3}$$

where $A_{ijc} = A_{ij} - K_{ij}$. Combined (3) with (2) shows that $u_{si}(t)$ is to stabilize the following CNHOFA-MAS as

$$x_i(t+n) + \sum_{j=0}^{n-1} A_{ijc} x_i(t+j) = 0 \tag{4}$$

and $v_i(t)$ is to implement the coordination performance. For coordination, a cost function is established as

$$J(t) = \sum_{i=1}^{N} J_i(t) \tag{5}$$

where $J_i(t)$ is a subcost function to measure the coordination relationship of the ith HOFA-MAS.

Problem 1: For HOFA-MAS (1) under Assumption 1, this research aims to present a predictive control strategy (2) to achieve simultaneous stability and output consensus, such that the following:

C1 for a known reference input $y_r(t)$, if $\|y_r(t)\| < \infty$, $\lim_{t\to\infty} \|y_i(t)\| < \infty, \forall i \in \mathcal{N}, \forall t \geq 0$;

C2 $\lim_{t\to\infty} \|y_i(t) - y_j(t)\| = 0, \forall i \in \mathcal{N}, \forall j \in \mathcal{N}_i$.

III. Main Results

A. Solutions of K_{ij}

In this study, it is important to realize the stabilization of CNHOFA-MAS (4), which provides a better basis for coordination of closed-loop HOFA-NMAS (3). Based our presented result in [35], a parametric method to obtain the solutions of K_{ij} is given in Lemma 1.

Lemma 1 (see[35]): There are two ploynomial matrices $D_1(z)$, $D_2(z) \in \mathbb{R}^{n_i \times n_i}[z]$ satisfied

$$A_i(z) D_1(z) = D_2(z), A_i(z) = z^n + \sum_{j=0}^{n-1} A_{ij} z^j$$

with $D_i(z) = \sum_{j=0}^{\epsilon} D_{ij} z^j$. Denote $D_i(z) = [d_{jl}^i(z)]_{n_i \times n_i}$, $i = 1, 2$, then $\epsilon = \max\{\deg(d_{jl}^i(z)), j, l = 1, 2, \ldots, n_i\}$, such that $K_i = [\, K_{i0} \; K_{i1} \cdots K_{i(n-1)} \,]$ is calculated by $K_i = W_i V_{ic}^{-1}$ with

$$V_i = \sum_{j=0}^{\epsilon} D_{1i} Z_i \Lambda_i^j, W_i = \sum_{j=0}^{\epsilon} D_{2i} Z_i \Lambda_i^j$$

$$V_{ic} = \left[V_i^{\mathrm{T}} \; \Lambda_i^{\mathrm{T}} V_i^{\mathrm{T}} \cdots (\Lambda_i^{n-1})^{\mathrm{T}} V_i^{\mathrm{T}} \right]^{\mathrm{T}}$$

where Λ_i is a Schur matrix and Z_i is an arbitrary matrix to offer design degrees of freedom.

B. Optimal Design of Predictive Increment

Denote $q^j x_i(t) = x_i(t+j)$, $j \in \mathbb{Z}$, then system (3) is further expressed as

$$A_i(q^{-1}) x_i(t) = B_i(q^{-1}) v_i(t-1) \tag{6}$$

where $A_i(q^{-1}) = I + \sum_{j=0}^{n-1} A_{ijc} q^{j-n}$ and $B_i(q^{-1}) = q^{1-n}$. Then, a Diophantine equation is introduced as

$$I = E_{i,j}(q^{-1}) A_i \Delta + q^{-j} F_{i,j}(q^{-1}) \tag{7}$$

where $\Delta = 1 - q^{-1}$, $E_{i,j}$ and $F_{i,j}$ are polynomial matrices decided by $A_i(q^{-1})$ and prediction horizon j, that is

$$E_{i,j}(q^{-1}) = e_{i,j,0} + e_{i,j,1} q^{-1} + \cdots + e_{i,j,j-1} q^{-(j-1)}$$

$$F_{i,j}(q^{-1}) = f_{i,j,0} + f_{i,j,1} q^{-1} + \cdots + f_{i,j,n} q^{-n}.$$

Multiplying $E_{i,j} \Delta q^j$ at both side of (6) has

$$E_{i,j} A_i \Delta x_i(t+j) = E_{i,j} B_i \Delta v_i(t+j-1)$$

combined with (7), the abovementioned is transformed as

$$x_i(t+j) = F_{i,j} x_i(t) + E_{i,j} B_i \Delta v_i(t+j-1).$$

Denote $G_{i,j} = E_{i,j} B_i$ where $G_{i,j}(q^{-1}) = g_{i,j,0} + g_{i,j,1} q^{-1} + \cdots + g_{i,j,j-1} q^{-(n+j-2)}$, then an incremental HOFA prediction model is constructed as

$$x_i(t+j) = F_{i,j} x(t) + G_{i,j} \Delta v_i(t+j-1). \tag{8}$$

To determine the $\Delta v_i(t)$, $J_i(t)$ in (5) is established as

$$\begin{aligned} J_i(t) = &\sum_{j\in\mathcal{N}_i} a_{ij}\|\hat{Y}_i(t+N_y|t) - \hat{Y}_j(t+N_y|t)\|^2 \\ &+ b_i\|\hat{Y}_i(t+N_y|t) - Y_r(t+N_y)\|^2 \\ &+ c_i\|\Delta\hat{V}_i(t+N_u|t)\|^2 \end{aligned} \tag{9}$$

with

$$\begin{aligned} \hat{Y}_i(t+N_y|t) &= \left[\hat{y}_i^{\mathrm{T}}(t+N_y|t)\ \cdots\ \hat{y}_i^{\mathrm{T}}(t+1|t)\right]^{\mathrm{T}} \\ Y_r(t+N_y) &= \left[y_r^{\mathrm{T}}(t+N_y)\ \cdots\ y_r^{\mathrm{T}}(t+1)\right]^{\mathrm{T}} \\ \Delta\hat{V}_i(t+N_u|t) &= \left[\Delta\hat{v}_i^{\mathrm{T}}(t+N_u|t)\ \cdots\ \Delta\hat{v}_i^{\mathrm{T}}(t|t)\right]^{\mathrm{T}} \end{aligned}$$

where $\hat{y}_i(t+j|t)$, $j=1,2,\ldots,N_y$ and $\Delta\hat{v}_i(t+j|t)$, $j=1,2,\ldots,N_u$ are the jth ahead predictions of $y_i(t)$ and $\Delta v_i(t)$, $Y_r(t+N_y)$ is the known reference input, N_y and N_u are prediction horizons of output and control, $a_{ij}\geqq 0$ is the (i,j)th element of adjacent matrix $\mathcal{A}$, b_i and c_i are weighting factors and positive numbers. In (9), the first part focuses on the coordination performance of HOFA-MASs, the second part pays attention to the difference between the reference input and output prediction, and the third one proposes a constraint on the change of predictive increment, which is benefit to improve the coordination performance and limit the amplitude and rate of changes of control input.

From (8), $x_i(t)$ can be predicted as

$$\begin{aligned} \hat{x}_i(t+1|t) &= F_{i,1}x_i(t) + G_{i,1}\Delta\hat{v}_i(t|t) \\ &\vdots \\ \hat{x}_i(t+k|t) &= F_{i,k}x_i(t) + G_{i,k}\Delta\hat{v}_i(t+k-1|t) \end{aligned}$$

considering (1), output prediction is provided as

$$\hat{y}_i(t+k|t) = C_i\hat{x}_i(t+k|t) \tag{10}$$

for $k=N_u+1,N_u+2,\ldots,N_y$, $\hat{v}_i(t+k|t)=\hat{v}_i(t+N_u|t)$, that is, $\Delta\hat{v}_i(t+k|t)=0$, so that (10) can be compactly formulated as

$$\hat{Y}_i(t+N_y|t) = P_{i1}x_i(t) + P_{i2}\Delta\hat{V}_i(t+N_u|t) \tag{11}$$

where

$$P_{i1} = C_i\begin{bmatrix} F_{i,N_y} \\ \vdots \\ F_{i,N_u+1} \\ F_{i,N_u} \\ \vdots \\ F_{i,1} \end{bmatrix}, P_{i2} = C_i\begin{bmatrix} G_{i,N_y} & 0 & \cdots & 0 \\ \vdots & \vdots & \cdots & \vdots \\ G_{i,N_u+1} & 0 & \cdots & 0 \\ 0 & G_{i,N_u} & \ddots & \vdots \\ \vdots & \ddots & \ddots & 0 \\ 0 & \cdots & 0 & G_{i,1} \end{bmatrix}.$$

Moreover, define an incremental constraint as

$$\Delta\hat{v}_i(t+j|t) = \gamma_{ij}I\Delta\hat{v}_i(t|t) \tag{12}$$

where $\gamma_{ij}>0$, $j=1,2,\ldots,N_u$, is the weighting factor, then P_{i2} is degenerated as

$$P_{i3} = P_{i2}\Gamma_i, \Gamma_i = \text{Blockdiag}\{\gamma_{iN_u}I,\ldots,\gamma_{i1}I,I\}. \tag{13}$$

To solve the optimal solution of $\Delta v_i(t)$, let

$$\frac{\partial}{\partial\Delta\hat{V}_i(t+N_u|t)}J(t) = 0, i\in\mathcal{N}$$

combined with (11) has

$$\begin{aligned} &\sum_{j\in\mathcal{N}_i} a_{ij}P_{i3}^{\mathrm{T}}(P_{i1}x_i(t) + P_{i3}\Delta\hat{V}_i(t+N_u|t) - P_{j1}x_j(t) \\ &- P_{j3}\Delta\hat{V}_j(t+N_u|t)) + b_iP_{i3}^{\mathrm{T}}(P_{i1}x_i(t) + P_{i3}\Delta\hat{V}_i(t+N_u|t) \\ &- Y_r(t+N_y)) + c_i\Delta\hat{V}_i(t+N_u|t) = 0 \end{aligned}$$

then

$$\Delta\hat{V}(t+N_u|t) = M^{-1}Qx(t) + M^{-1}SY_r(t+N_y)$$

where

$$\begin{aligned} \Delta\hat{V}(t+N_u|t) &= \left[\Delta\hat{V}_1^{\mathrm{T}}(t+N_u|t)\cdot\Delta\hat{V}_N^{\mathrm{T}}(t+N_u|t)\right]^{\mathrm{T}} \\ x(t) &= \left[x_1^{\mathrm{T}}(t)\ \cdots\ x_N^{\mathrm{T}}(t)\right]^{\mathrm{T}} \end{aligned}$$

and

$$\begin{aligned} &M = \{m_{ij}\}, m_{ii} = (a_i+b_i)P_{i3}^{\mathrm{T}}P_{i3} + c_iI, m_{ij} = -a_{ij}P_{i3}^{\mathrm{T}}P_{j3} \\ &Q = \{q_{ij}\}, q_{ii} = -(a_i+b_i)P_{i3}^{\mathrm{T}}P_{i1}, q_{ij} = a_{ij}P_{i3}^{\mathrm{T}}P_{j1} \\ &S = \left[b_1P_{13}\ \cdots\ b_NP_{N3}\right]^{\mathrm{T}}, a_i = \sum_{j\in\mathcal{N}_i} a_{ij} \end{aligned}$$

further the predictive increment of the ith HOFA-MAS is set to

$$\begin{aligned} \Delta v_i(t) = \Delta\hat{v}_i(t|t) &= H_i\Delta\hat{V}(t+N_u|t) \\ &= H_iM^{-1}Qx(t) + H_iM^{-1}SY_r(t+N_y) \end{aligned} \tag{14}$$

where $H_i\in\mathbb{R}^{n_i\times(N_u+1)\tilde{n}}$ is a zero matrix expect the $(N_u+1)i$th column is an unit matrix with $\tilde{n}=\sum_{i=1}^{N}n_i$, and M, Q, and S are design coefficients of predictive increment. Then, the predictive control strategy (2) can be further developed as

$$\begin{aligned} u_i(t) &= B_i^{-1}(u_{si}(t) + v_i(t)) \\ &= B_i^{-1}\sum_{j=0}^{n-1}K_{ij}x_i(t+j) + B_i^{-1}v_i(t-1) \\ &\quad + B_i^{-1}H_iM^{-1}Qx(t) + B_i^{-1}H_iM^{-1}SY_r(t+N_y). \end{aligned}$$

C. Analysis of Simultaneous Stability and Output Consensus

Without loss of generality, assume that $y_r(\cdot)=y_r$, and denote $A_{ic}=A_i^{-1}(q^{-1})B_i(q^{-1})$, combined (6) with (14) has

$$\begin{aligned} \Delta x_i(t+1) &= A_{ic}\Delta v_i(t) \\ &= A_{ic}H_iM^{-1}Qx(t) + H_iM^{-1}SY_r(t+N_y) \end{aligned}$$

let $\Delta x(t) = [\Delta x_1^{\mathrm{T}}(t)\ \cdots\ \Delta x_N^{\mathrm{T}}(t)]^{\mathrm{T}}$, then

$$\begin{aligned} \Delta x(t+1) &= A_Qx(t) + A_SY_r(t+N_y) \\ &= (A_Q+I)\Delta x(t) \end{aligned} \tag{15}$$

where

$$A_Q = \begin{bmatrix} A_{1c}H_1M^{-1}Q \\ \vdots \\ A_{Nc}H_NM^{-1}Q \end{bmatrix}, A_S = \begin{bmatrix} A_{1c}H_1M^{-1}S \\ \vdots \\ A_{Nc}H_NM^{-1}S \end{bmatrix}.$$

Theorem 1: The closed-loop HOFA-MAS (3) is simultaneous stable and output consensus if and only if system (15) is asymptotically stable.

Proof: Sufficiency. If the closed-loop HOFA-MAS (3) realizes the simultaneous stability and output consensus, Conditions C1 and C2 in Problem 1 are held, such that $\Delta x_i(t) \to 0$ as $t \to \infty$, that is, $\Delta x(t) \to 0$ as $t \to \infty$. Thus, system (15) is asymptotically stable.

Necessity. If system (15) is asymptotically stable, $\Delta x(t) \to 0$ as $t \to \infty$. On the one hand, it means the closed-loop HOFA-MAS (3) is bounded stable, such that Condition C1 in Problem 1 is held. On the other hand, it results in $\Delta v(t) \to 0$ as $t \to \infty$. Combining (11) with (12) and (13) has

$$\hat{Y}_i(t+N_y|t) = P_{i1}x_i(t) + P_{i3}\Delta\hat{V}_i(t|t)$$

where $\Delta\hat{V}_i(t|t) = [\,\Delta\hat{v}_i^{\mathrm{T}}(t|t) \cdots \Delta\hat{v}_i^{\mathrm{T}}(t|t)\,]^{\mathrm{T}}$. Due to $\Delta v(t) = 0$, $\Delta\hat{V}_i(t|t) = 0$, then $\hat{Y}_i(t+N_y|t) = P_{i1}x_i(t)$. Meanwhile, considering (14) yields that $Qx(t) + SY_r(t+N_y) = 0$, which derives

$$\begin{bmatrix} q_{11} & q_{12} & \cdots & q_{1N} \\ q_{21} & q_{22} & \cdots & q_{2N} \\ \vdots & \vdots & \ddots & \vdots \\ q_{N1} & q_{N2} & \cdots & q_{NN} \end{bmatrix} \begin{bmatrix} x_1(t) \\ x_2(t) \\ \vdots \\ x_N(t) \end{bmatrix} + \begin{bmatrix} b_1P_{13}^{\mathrm{T}} \\ b_2P_{23}^{\mathrm{T}} \\ \vdots \\ b_NP_{N3}^{\mathrm{T}} \end{bmatrix} Y_r(t+N_y) = 0.$$

Concretely, it results in

$$\sum_{j\in\mathcal{N}_i} a_{ij}P_{i3}^{\mathrm{T}}\hat{Y}_j(t+N_y) + b_iP_{i3}^{\mathrm{T}}Y_r(t+N_y) - (a_i+b_i)P_{i3}^{\mathrm{T}}\hat{Y}_i(t+N_y) = 0$$

that is

$$\sum_{j\in\mathcal{N}_i} a_{ij}P_{i3}^{\mathrm{T}}\left(\hat{Y}_j(t+N_y) - \hat{Y}_i(t+N_y)\right) + b_iP_{i3}^{\mathrm{T}}\left(Y_r(t+N_y) - \hat{Y}_i(t+N_y)\right) = 0$$

further

$$\sum_{j\in\mathcal{N}_i} a_{ij}\left(\hat{Y}_j(t+N_y) - Y_r(t+N_y)\right) - (a_i+b_i)\left(\hat{Y}_i(t+N_y) - Y_r(t+N_y)\right) = 0$$

which can be converted as

$$\begin{bmatrix} -(a_1+b_1)I & \cdots & a_{1N}I \\ \vdots & \ddots & \vdots \\ a_{N1}I & \cdots & -(a_N+b_N)I \end{bmatrix} \times \begin{bmatrix} \hat{Y}_1(t+N_y) - Y_r(t+N_y) \\ \vdots \\ \hat{Y}_N(t+N_y) - Y_r(t+N_y) \end{bmatrix} = 0$$

such that $Y_r(t+N_y) = \hat{Y}_i(t+N_y)$, $\forall i \in \mathcal{N}$, which leads to $\hat{Y}_i(t+N_y) = \hat{Y}_j(t+N_y)$, $\forall i \in \mathcal{N}$, $j \in \mathcal{N}_i$. When $N_y \to \infty$,

$$\lim_{t\to\infty} \|y_i(t) - y_j(t)\| = 0, \forall i \in \mathcal{N} \quad \forall j \in \mathcal{N}_i$$

then Condition C2 in Problem 1 is satisfied. Hence, the closed-loop HOFA-MAS (3) implements the simultaneous stability and output consensus. Moreover, Lemma 2 is provided to judge the asymptotic stability of system (15).

Lemma 2 (see[36]): System (15) is asymptotically stable if and only if there exists a Lyapunov function $V(\Delta x(t))$ such that

1) $V(\Delta x(t))$ is positive definite;
2) $\Delta V(\Delta x(t)) = V(\Delta x(t+1)) - V(\Delta x(t))$ is negative definite.

□

Remark 1: The feasibility of the proposed algorithm is discussed for two aspects. One is to obtain the optimal solution of $\Delta v_i(t)$, another is to guarantee the simultaneous stability and output consensus. The optimal solution of $\Delta v_i(t)$ is obtained by minimizing $J(t)$ in (5) and (9), that is

$$\frac{\partial}{\partial\Delta\hat{V}_i(t+N_u|t)} J(t) = 0, i \in \mathcal{N}.$$

It is obvious that each feasible solution for t time is also applicable at $t+\mu$ time, $\forall\mu > 0$. Thus, $\Delta v_i(t)$ is feasible at $t+\mu$ time, $\forall\mu > 0$, when it is applicable for t time. The simultaneous stability and output consensus has been analyzed in Theorem 1. Then, Algorithm 1 is provided to solve the proposed control law.

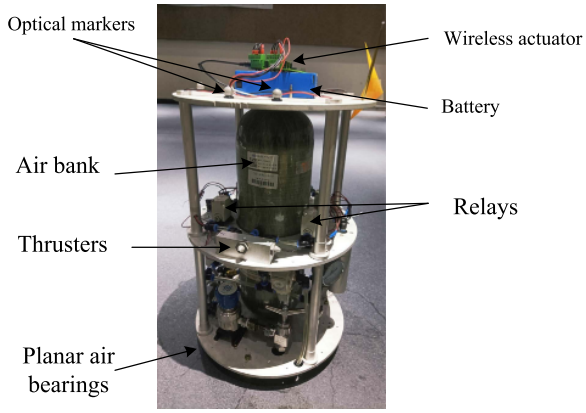

Fig. 2. Hardware of ABS.

IV. Formation Control of Air-Bearing Simulators

A. System Description

Air-bearing simulator (ABS), whose hardware is shown in Fig. 2, is used to simulate the motion and control of spacecrafts under microgravity environment on the ground, such as rendezvous and docking, flying-around, formation, and so on,

Algorithm 1: Solve the Predictive Control Strategy (2).

Input: A_{ij}, B_i, C_i

Output: $K_{ij}, \Delta v_i(t)$

1) Obtain two polynomial matrices $D_1(z)$ and $D_2(z)$ as

$$D_1(z) = \text{adj}\,(A_i(z))\,, D_2(z) = \det\,(A_i(z))\,I.$$

2) Choose parameter Z_i and Schur matrix Λ_i to compute V_i and W_i, that is,

$$V_i = \sum_{j=0}^{\epsilon} D_{1i} Z_i \Lambda_i^j, W_i = \sum_{j=0}^{\epsilon} D_{2i} Z_i \Lambda_i^j,$$

$$V_{ic} = \left[V_i^{\mathrm{T}} \ \Lambda_i^{\mathrm{T}} V_i^{\mathrm{T}} \ \cdots \ (\Lambda_i^{n-1})^{\mathrm{T}} V_i^{\mathrm{T}} \right]^{\mathrm{T}}.$$

3) Calculate the coefficient matrix $K_i = W_i V_{ic}^{-1}$.

4) Use a Diophantine Equation (7) to construct an incremental HOFA prediction model (8), and obtain the relative output prediction (11).

5) Choose a_{ij}, b_i, c_i and γ_{ij} to optimize the $J(t)$ in (5) and (9), so that M, Q and S are obtained as

$$M = \{m_{ij}\}, Q = \{q_{ij}\},$$

$$m_{ii} = (a_i + b_i) P_{i3}^{\mathrm{T}} P_{i3} + c_i I, m_{ij} = -a_{ij} P_{i3}^{\mathrm{T}} P_{j3},$$

$$q_{ii} = -(a_i + b_i) P_{i3}^{\mathrm{T}} P_{i1}, q_{ij} = -a_{ij} P_{i3}^{\mathrm{T}} P_{j1},$$

$$S = \left[b_1 P_{13} \ \cdots \ b_N P_{N3} \right]^{\mathrm{T}}, a_i = \sum_{j \in \mathcal{N}_i} a_{ij}.$$

6) Compute the predictive increment $\Delta v_i(t)$ by (14).

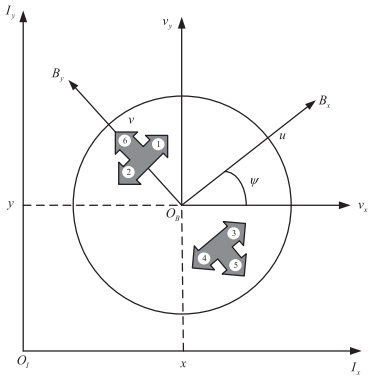

Fig. 3. Coordinate systems and distribution of six gas thrusters.

which has attracted great interests of researchers (see [37]–[40]). For the ABS, the relative coordinates are given in Fig. 3, where $F - O_I I_x I_y$ and $F - O_B B_x B_y$ are the inertial and body coordinate systems. In fact, ABS has three controllable degrees of freedom, that is, x, y, and ψ components in $F - O_I I_x I_y$ coordinate, and ψ also establishes a relationship between $F - O_I I_x I_y$ and $F - O_B B_x B_y$ coordinates. The experimental platform is shown in Fig. 4, where VICON Infrared Cameras obtain the data of x, y, and ψ by means of optical makers of ABSs, and transmit them into VICON Server. Android Controller applies these state conditions to compute the control inputs, and Computer

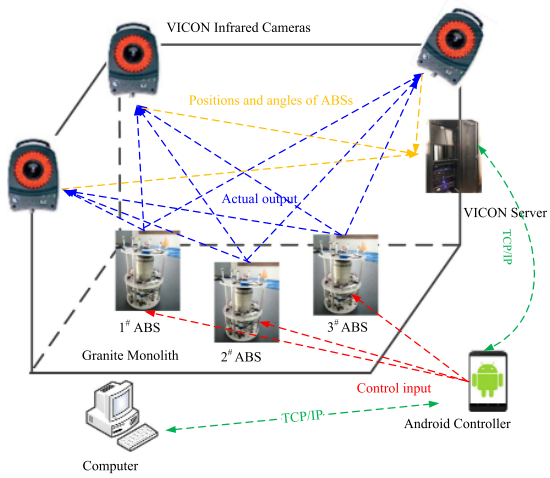

Fig. 4. Experimental platform.

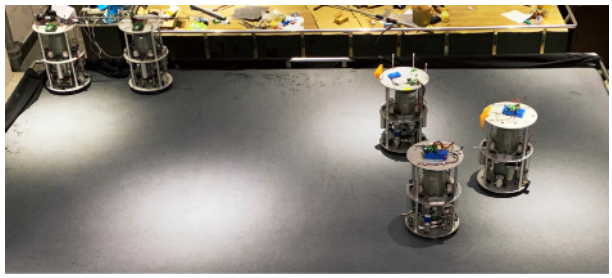

Fig. 5. Experimental environment.

TABLE I
RELATIVE PARAMETERS OF ABSS

Parameter	Notation	Value
Mass	m_i	19.4 kg
Moment of inertia	J_i	0.185 kg · m^2
Radius	r_i	0.18 m
Sampling period	T	0.2 s

is used to monitor and save the real-time data. The practical experimental environment is shown in Fig. 5. The relative parameters of ABSs are shown in Table I, where $i = 1, 2, 3$ indicates $1^{\#}$, $2^{\#}$, and $3^{\#}$ ABS. In our experimental platform, three ABSs are operated in the local area network (LAN). The Ping delay of LAN is between 30 and110 ms by testing. To avoid the influences of packets loss and delays on experiments and to calculate easily, the sampling period is chosen as 0.2 s. Meanwhile, Simulink models can be transformed into the C programs via Simulink Coder, which can be complied, linked, and run on Android by NDK and other software. The control programs in Android controller perform in Linux kernel instead of Android virtual machine and use C program rather than Java, which ensures the real-time communication between Android controller and wireless actuator via TCP/IP protocol, the details are reported by our team in [41]. Netconview, designed by our team (see [42]), is a real-time supervisory control software for networked control systems on computer side, which can realize the real-time monitoring and data saving.

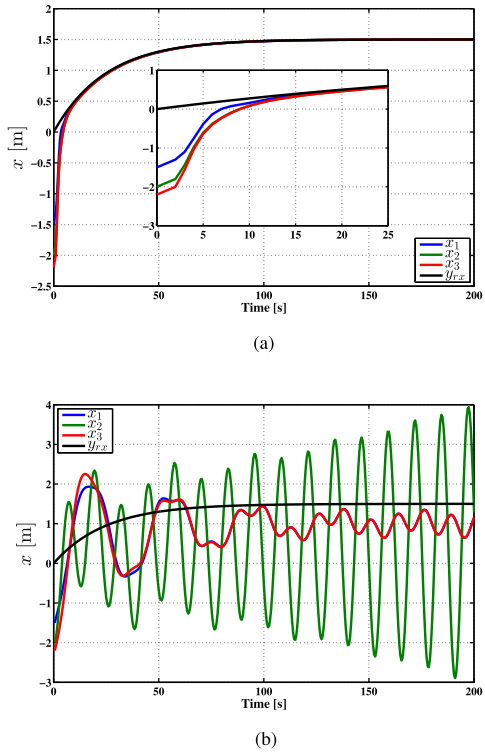

Fig. 6. Comparison between the proposed strategy and Xi. (a) Coordinated control of system (17a) based on (18). (b) Coordinated control of system (17a) based on Xi.

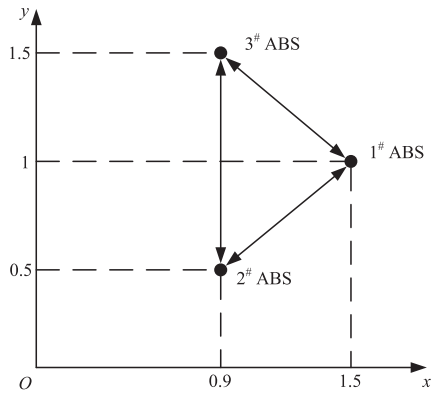

Fig. 7. Desired formation of three ABSs.

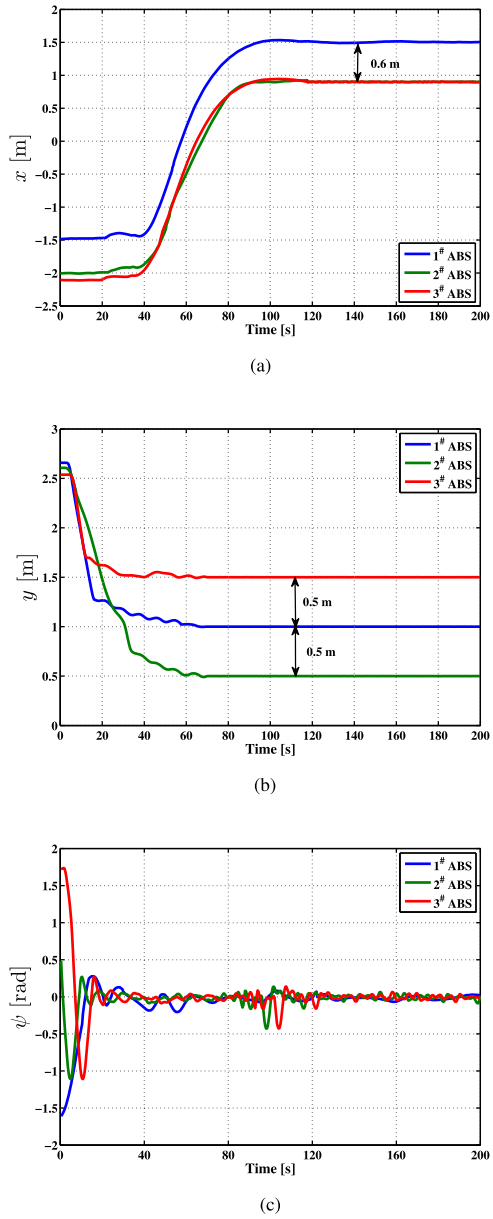

Fig. 8. States responses of formation control of three ABSs. (a) Position responses of formation control on x-axis. (b) Position responses of formation control on y-axis. (c) Angle responses of formation control on ψ-axis.

Assume that the origin of $F-O_I I_x I_y$ coordinate is located in the center of granite monolith, the dynamical models of the ith ABS are

$$m_i\ddot{x}_i = F_{xi}, m_i\ddot{y}_i = F_{yi}, J_i\ddot{\psi} = F_{Ti} \tag{16}$$

where F_{xi}, F_{yi}, and F_{Ti} are the thrust and torque of the ith ABS. Based on the discretization of system (16), a group of second-order fully actuated systems is established as

$$m_i x_i(t+2) - 2m_i x_i(t+1) + m_i x_i(t) = T^2 F_{xi}(t) \tag{17a}$$

$$m_i y_i(t+2) - 2m_i y_i(t+1) + m_i x_i(t) = T^2 F_{yi}(t) \tag{17b}$$

$$J_i\psi(t+2) - 2J_i\psi(t+1) + J_i\psi(t) = T^2 F_{Ti}(t). \tag{17c}$$

B. Simulation Comparison

Take system (17a) as an example to compare with the standard model predictive control in [43]. Let $a_{ii}=0$, $a_{ij}=1$, $b_i=1$, $c_i=0.01$, $i,j=1,2,3$.

For the proposed work, a predictive control for system (17a) is proposed as

$$F_{xi}(t) = \frac{1}{T^2}K_{i0}x_i(t) + \frac{1}{T^2}K_{i1}x_i(t+1) + \frac{1}{T^2}v_i(t) \tag{18}$$

where $K_{i0}=19.0159$ and $K_{i1}=-19.2060$. Then, the closed-loop form of system (17a) is formulated as

$$m_i x_i(t+2) + A_{i1c}x_i(t+1) + A_{i0c}x_i(t) = v_i(t)$$

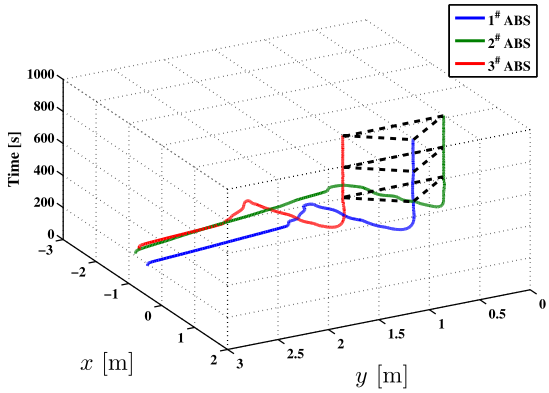

Fig. 9. Practical formation of three ABSs.

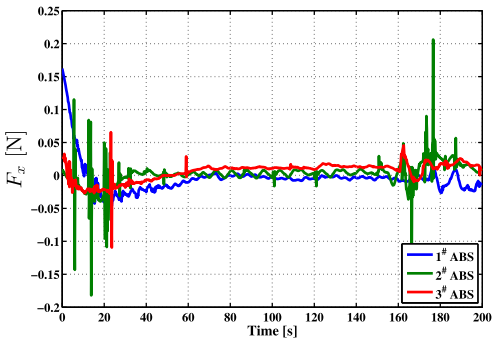

(a)

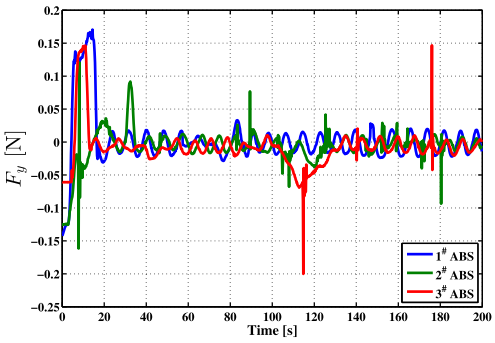

(b)

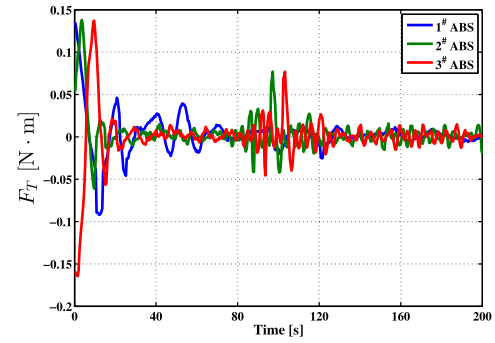

(c)

Fig. 10. Control inputs of formation control of three ABSs. (a) Control inputs of formation control on x-axis. (b) Control inputs of formation control on y-axis. (c) Control inputs of formation control on ψ-axis.

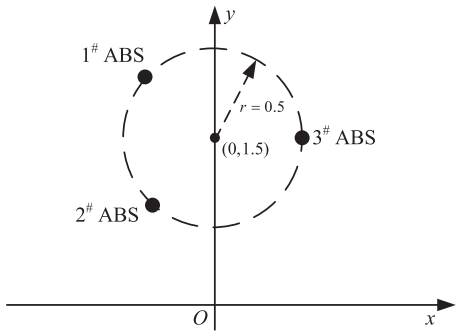

Fig. 11. Desired trajectory of three ABSs.

where $A_{i0c} = 0.3880$, $A_{i1c} = -19.7880$. For (6), $A_i(q^{-1}) = 1 - 1.02q^{-1} + 0.02q^{-2}$ and $B_i(q^{-1}) = 0.0515q^{-1}$ such that an incremental HOFA prediction model is established as (8). Choose $N_y = 5$, $N_u = 3$, $\Gamma_i = \text{diag}\{25, 24, 23, 1\}$, based on the solution of Diophantine equation in [44], $F_{i,j}$ and $G_{i,j}$ are obtained as $F_{i,1} = 2.02 - 1.04q^{-1} + 0.02q^{-2}$, $F_{i,2} = 3.0404 - 2.0808q^{-1} + 0.0404q^{-2}$, $F_{i,3} = 4.0608 - 3.1216q^{-1} + 0.0608q^{-2}$, $F_{i,4} = 5.0802 - 4.1624q^{-1} + 0.0812q^{-2}$, $F_{i,5} = 6.1016 - 5.2032q^{-1} + 0.1016q^{-2}$, $G_{i,1} = 0.0515q^{-1}$, $G_{i,2} = 0.0515q^{-1} + 0.1040q^{-2}$, $G_{i,3} = 0.0515q^{-1} + 0.1040q^{-2} + 0.1566q^{-3}$, $G_{i,4} = 0.0515q^{-1} + 0.1040q^{-2} + 0.1566q^{-3} + 0.2091q^{-4}$, $G_{i,5} = 0.0515q^{-1} + 0.1040q^{-2} + 0.1566q^{-3} + 0.2091q^{-4} + 0.2616q^{-5}$.

For Xi in [43], system (17a) should be first converted into a first-order form as

$$X_i(t+1) = A_i X_i(t) + B_i F_{xi}(t)$$

with $X_i(t) = \begin{bmatrix} x_i(t) \\ x_i(t+1) \end{bmatrix}$, $A_i = \begin{bmatrix} 0 & 1 \\ -1 & 2 \end{bmatrix}$, and $B_i = \begin{bmatrix} 0 \\ 0.0021 \end{bmatrix}$, and choose the same prediction horizons, then $\hat{X}_i(t+1|t) = A_i X_i(t) + B_i \hat{F}_{xi}(t|t)$, $\hat{X}_i(t+2|t) = A_i^2 X_i(t) + \sum_{j=0}^{1} A_i^j B_i \hat{F}_{xi}(t+1-j|t)$, $\hat{X}_i(t+3|t) = A_i^3 X_i(t) + \sum_{j=0}^{2} A_i^j B_i \hat{F}_{xi}(t+2-j|t)$, $\hat{X}_i(t+4|t) = A_i^4 X_i(t) + \sum_{j=0}^{3} A_i^j B_i \hat{F}_{xi}(t+3-j|t)$, $\hat{X}_i(t+5|t) = A_i^5 X_i(t) + \sum_{j=1}^{4} A_i^j B_i \hat{F}_{xi}(t+4-j|t) + B_i \hat{F}_{xi}(t+3|t)$, then the simulation results are given in Fig. 6.

Fig. 6 provides the comparison of the coordination performance between the proposed strategy and Xi. Fig. 6(a) shows the proposed control (18) can realize the coordination in dynamical and steady processes and track the reference input, but in Fig. 6(b), Xi only realizes the coordination of x_1 and x_3, and it cannot track the reference input. The reason that (18) results in a better performance is that (18) gives a local feedback to stabilize the CNHOFA-MAS such that closed-loop performance is effectively improved, then prediction model is based on the constructed closed-loop HOFA system, which is benefit to improve the coordination performance. However, Xi uses a reduced-order open-loop one to establish a prediction model and ignores the improvement of the closed-loop performance. The comparison fully illustrates the effectiveness and superiority of the proposed predictive control strategy.

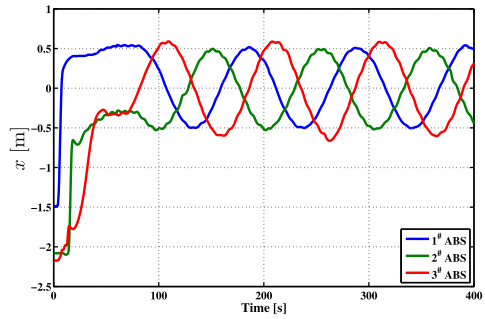

(a)

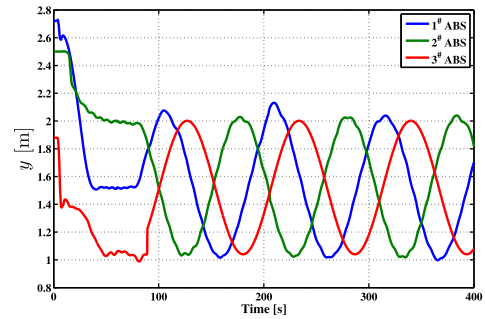

(b)

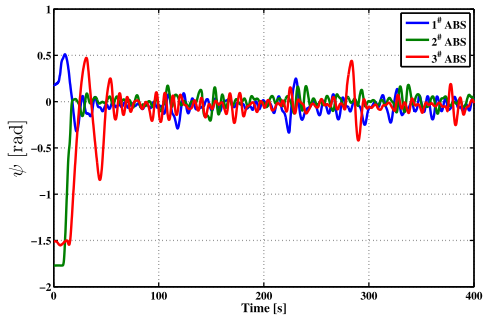

(c)

Fig. 12. States responses of flying-around of three ABSs. (a) Position responses of flying-around on x-axis. (b) Position responses of flying-around on y-axis. (c) Angle responses of flying-around on ψ-axis.

C. Experimental Results

Formation control based on output consensus is presented for three ABSs to further demonstrate the availability of the predictive control strategy. For systems (17a) and (17b), the control protocols choose the same as (18). For system (17c), there is no communication, that is, the prediction items are zeros, a stabilization control is considered as

$$F_{Ti}(t) = \frac{1}{T^2}K'_{i0}\psi_i(t) + \frac{1}{T^2}K'_{i1}\psi_i(t+1)$$

where $K'_{i0} = 0.1673$ and $K'_{i1} = -0.2151$. Then, two experiments are carried out to verify the theoretical result.

Experiment 1 (Fixed formation): In this case, an experiment of fixed formation of three ABSs is taken, the desired formation is given in Fig. 7. By using (18), the experimental results are given in Figs. 8–10 .

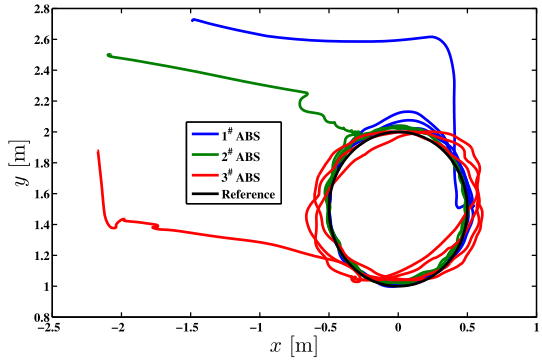

Fig. 13. Practical trajectory of three ABSs.

Fig. 8 shows the state responses of formation control of three ABSs, in Fig. 8(a) and (b), the position responses on x- and y-axis of three ABSs are almost the same and are changed coordinately, they also arrive at the pointed location simultaneously. Fig. 8(c) shows the angle responses on ψ-axis, which are stabilized effectively. The only drawback is that $\psi_i(t)$ exists the vibration phenomenon, the reasons are that there is airflow in the experimental site and the reaction forces produced by thrusters lead into the jitter. Fig. 9 is the practical formation of three ABSs. Combined Figs. 9 with 7 show that the proposed predictive control strategy can implement the desired formation and continue to follow it. Figs. 8 and 9 demonstrate the availability of the proposed predictive control strategy on formation control based on output consensus. The control inputs are shown in Fig. 10, where there exist disturbances because the dynamical model of ABS is after linearization and ignores some disturbances but control inputs need to cope with them.

Experiment 2 (Time-varying formation): Flying-around is a significant mission for noncooperative spacecrafts so that it is intensively considered in the literature (see [45]). In this case, an experiment of flying-around of three ABSs is taken, the desired circular trajectory is given in Fig. 11. By using (18), the experimental results are given in Figs. 12–14 . Meanwhile, let $i = 1$, the consensus errors on $x-$ and $y-$ axis are redefined as $\zeta_2^x(t) = x_2(t) - x_1(t) - d_{12}^x(t)$, $\zeta_3^x(t) = x_3(t) - x_1(t) - d_{13}^x(t)$, $\zeta_2^y(t) = y_2(t) - y_1(t) - d_{12}^y(t)$, $\zeta_3^y(t) = y_3(t) - y_1(t) - d_{13}^y(t)$, where $d_{1i}^x(t)$ and $d_{1i}^y(t)$, $i \in \mathcal{N}_1$ are time-variant formation variables, then the consensus errors are plotted in Fig. 15.

Fig. 12 shows the state responses of flying-around of three ABSs, in Fig. 12(a) and (b), the position responses on x- and y-axis of three ABSs reach the pointed locations within an allowable error, and then enter the expected orbit to operate the flying-around mission, the phases and amplitudes are changed cooperatively during the proposed task. Fig. 12(c) is the angle responses on ψ-axis, the reason that $\psi_i(t)$ exists the vibration phenomenon is analyzed in Experiment 1. Fig. 13 shows the practical trajectory of three ABSs, it implies the presented strategy can fly along the desired orbit within an allowable error and continue to follow it. Fig. 15 provides the consensus errors on $x-$ and y-axis to illustrate three ABSs have realized the dynamical coordination within a tolerance error, such that the availability of

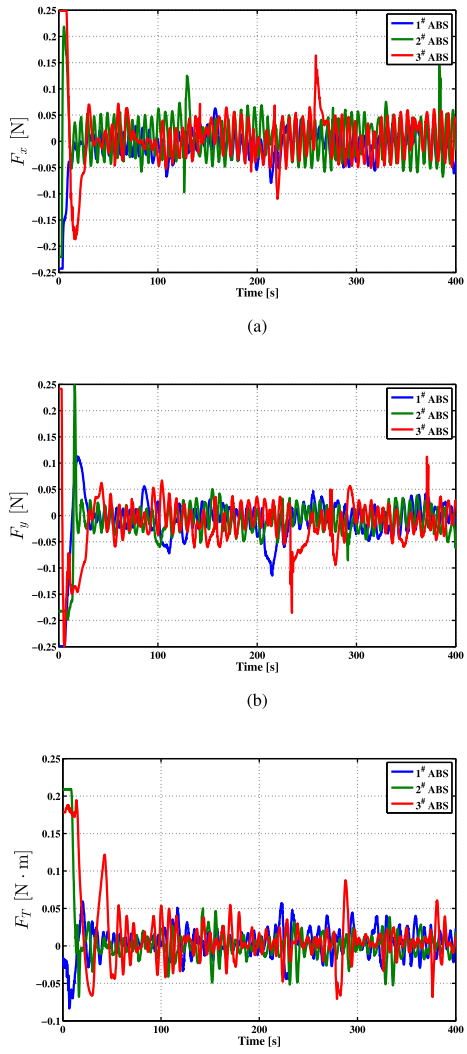

Fig. 14. Control inputs of flying-around of three ABSs. (a) Control inputs of flying-around on x-axis. (b) Control inputs of flying-around on y-axis. (c) Control inputs of flying-around on ψ-axis.

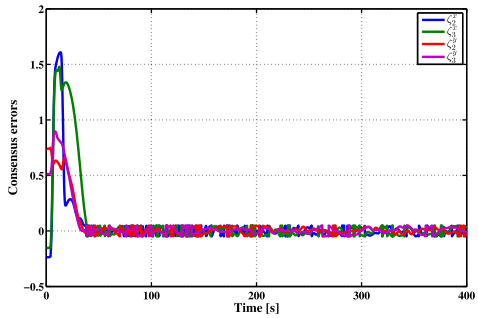

Fig. 15. Consensus errors on x- and y-axis.

the presented strategy on time-varying formation control based on output consensus is proved. Combining Figs. 13 and 15 with Fig. 11 propose there is difference between practical and desired trajectories, because both the linearized model ignores the uncertainties and nonlinearities and the interactions of three ABSs during the flying-around affect the dynamical consensus performance. It is also subject to the computing speed and limited computation resources of controller. The control inputs are given in Fig. 14, the reason why exists disturbances is also discussed in Experiment 1.

V. Conclusion

This research has investigated the coordinated control of HOFA-MASs with a predictive control strategy, which effectively implements the coordination performance and simultaneous stability and output consensus. A Diophantine equation has been used to establish an incremental HOFA prediction model, then a cost function has been minimized by the design of predictive control, thus, the optimal coordination controllers have been developed to realize the coordination performance of HOFA-MASs. Furthermore, a simple criterion has been constructed to ensure simultaneous stability and output consensus of the closed-loop HOFA-MASs. The future work might focus on the coordinated control of HOFA-MASs subject to some network constraints, such as network delays, packet dropouts, cyber attacks, and so on.

References

[1] F. Li, J. Qin, and Y. Kang, "Multi-agent system based distributed pattern search algorithm for non-convex economic load dispatch in smart grid," *IEEE Trans. Power Syst.*, vol. 34, no. 3, pp. 2093–2102, May 2019.

[2] K. Belkacem, K. Munawar, and S. S. Muhammad, "Distributed cooperative control of autonomous multi-agent UAV systems using smooth control," *J. Syst. Eng. Electron.*, vol. 31, no. 6, pp. 1297–1307, 2020.

[3] G. F. A. Martins and A. B. de Almeida, "Automatic power restoration in distribution systems modeled through multiagent systems," *IEEE Latin America Trans.*, vol. 18, no. 10, pp. 1768–1776, Oct. 2020.

[4] M. S. Rahman, S. S. T. Orchi, and M. E. Haque, "Cooperative multiagent based distributed power sharing strategy in low-voltage microgrids," *IEEE Trans. Ind. Appl.*, vol. 56, no. 4, pp. 3285–3296, Jul./Aug. 2020.

[5] B. Mu and Y. Shi, "Distributed LQR consensus control for heterogeneous multiagent systems: Theory and experiments," *IEEE/ASME Trans. Mechatronics*, vol. 23, no. 1, pp. 434–443, Feb. 2018.

[6] Q. M. Ta and C. C. Chea, "Multi-agent control for stochastic optical manipulation systems," *IEEE/ASME Trans. Mechatronics*, vol. 25, no. 4, pp. 1971–1979, Aug. 2020.

[7] W. Liu, S. Liu, J. Cao, Q. Wang, X. Lang, and T. Liu, "Learning communication for cooperation in dynamic agent-number environment," *IEEE/ASME Trans. Mechatronics*, vol. 26, no. 4, pp. 1846–1857, Aug. 2021.

[8] K. Li, C. C. Hua, X. You, and X. P. Guan, "Output feedback-based consensus control for nonlinear time delay multiagent systems," *Automatica*, vol. 111, 2020, Art. no. 108669.

[9] L. Tan, C. Li, J. Huang, and T. Huang, "Output feedback leader-following consensus for nonlinear stochastic multiagent systems: The event-triggered method," *Appl. Math. Computation*, vol. 395, 2021, Art. no. 125879.

[10] H. Wang, W. Ren, W. Yu, and D. Zhang, "Fully distributed consensus control for a class of disturbed second-order multi-agent systems with directed networks," *Automatica*, vol. 132, 2021, Art. no. 109816.

[11] H. Tan, Z. Miao, Y. Wang, M. Wu, and Z. Huang, "Data-driven distributed coordinated control for cloud-based model-free multiagent systems with communication constraints," *IEEE Trans. Circuits Syst. I: Regular Papers*, vol. 67, no. 9, pp. 3187–3198, Sep. 2020.

[12] B. Cheng and Z. Li, "Coordinated tracking control with asynchronous edge-based event-triggered communications," *IEEE Trans. Autom. Control*, vol. 64, no. 10, pp. 4321–4328, Oct. 2019.

[13] F. Mehdifar, C. P. Bechlioulis, F. Hashemzadeh, and M. Baradarannia, "Prescribed performance distance-based formation control of multi-agent systems," *Automatica*, vol. 119, 2020, Art. no. 109086.

[14] V. Rezaei and M. Stefanovic, "Event-triggered cooperative stabilization of multiagent systems with partially unknown interconnected dynamics," *Automatica*, vol. 130, 2021, Art. no. 109657.
[15] Z. Sun, N. Huang, B. D. O. Anderson, and Z. Duan, "Event-based multiagent consensus control: Zeno-free triggering via $\mathcal{L}^p$ signals," *IEEE Trans. Cybern.*, vol. 50, no. 1, pp. 284–296, Jan. 2020.
[16] B. Wang, W. Chen, J. Wang, B. Zhang, Z. Zhang, and X. Qiu, "Cooperative tracking control of multiagent systems: A heterogeneous coupling network and intermittent communication framework," *IEEE Trans. Cybern.*, vol. 49, no. 12, pp. 4308–4320, Aug. 2019.
[17] Q. Shen, P. Shi, J. Zhu, S. Wang, and Y. Shi, "Neural networks-based distributed adaptive control of nonlinear multiagent systems," *IEEE Trans. Neural Netw. Learn. Syst.*, vol. 31, no. 3, pp. 1010–1021, Mar. 2020.
[18] Q. Shen, Y. Shi, R. Jia, and P. Shi, "Design on type-2 fuzzy-based distributed supervisory control with backlash-like hysteresis," *IEEE Trans. Fuzzy Syst.*, vol. 29, no. 2, pp. 252–261, Feb. 2021.
[19] W. Zou, P. Shi, Z. Xiang, and Y. Shi, "Finite-time consensus of second-order switched nonlinear multi-agent systems," *IEEE Trans. Neural Netw. Learn. Syst.*, vol. 31, no. 5, pp. 1757–1762, May 2020.
[20] R. Manivannan, R. Samidurai, J. Cao, and M. Perc, "Design of resilient reliable dissipativity control for systems with actuator faults and probabilistic time-delay signals via sampled-data approach," *IEEE Trans. Syst., Man, Cybern. Syst.*, vol. 50, no. 11, pp. 4243–4255, Nov. 2020.
[21] G. P. Liu, "Coordinated control of networked multiagent systems with communication constraints using a proportional integral predictive control strategy," *IEEE Trans. Cybern.*, vol. 50, no. 11, pp. 4735–4743, Nov. 2020.
[22] G. P. Liu, "Predictive control of networked nonlinear multiagent systems with communication constraints," *IEEE Trans. Syst., Man, Cybern. Syst.*, vol. 50, no. 11, pp. 4447–4457, Nov. 2020.
[23] Z. H. Pang, W. C. Luo, G. P. Liu, and Q. L. Han, "Observer-based incremental predictive control of networked multi-agent systems with random delays and packet dropouts," *IEEE Trans. Circuits Syst. II: Express Briefs*, vol. 68, no. 1, pp. 426–430, Jan. 2021.
[24] H. Yang, S. Ju, Y. Xia, and J. Zhang, "Predictive cloud control for networked multiagent systems with quantized signals under dos attacks," *IEEE Trans. Syst., Man, Cybern. Syst.*, vol. 51, no. 2, pp. 1345–1353, Feb. 2021.
[25] G. Franzè, F. Tedesco, and D. Famularo, "Resilience against replay attacks: A distributed model predictive control scheme for networked multi-agent systems," *IEEE/CAA J. Automatica Sinica*, vol. 8, no. 3, pp. 628–640, Mar. 2021.
[26] L. Li, P. Shi, R. K. Agarwal, C. K. Ahn, and W. Xing, "Event-triggered model predictive control for multiagent systems with communication constraints," *IEEE Trans. Syst., Man, Cybern. Syst.*, vol. 51, no. 5, pp. 3304–3316, May 2021.
[27] Q. Wang, Z. Duan, Y. Lv, Q. Wang, and G. Chen, "Distributed model predictive control for linear-quadratic performance and consensus state optimization of multiagent systems," *IEEE Trans. Cybern.*, vol. 51, no. 6, pp. 2905–2915, Jun. 2021.
[28] D. K. Gu and D. W. Zhang, "Parametric control to second-order linear time-varying systems based on dynamic compensator and multi-objective optimization," *Appl. Math. Computation*, vol. 365, 2020, Art. no. 124681.
[29] D. K. Gu and D. W. Zhang, "A parametric method to design dynamic compensator for high-order quasi-linear systems," *Nonlinear Dyn.*, vol. 100, no. 2, pp. 1379–1400, 2020.
[30] G. R. Duan, "High-order fully actuated systems approaches: Part i. models and basic procedure," *Int. J. Syst. Sci.*, vol. 52, no. 2, pp. 422–435, 2021.
[31] G. R. Duan, "High-order system approaches: I fully-actuated systems and parametric designs," *ACTA Automatica Sinica*, vol. 46, no. 7, pp. 1333–1345, 2020.
[32] G. R. Duan, "High-order fully actuated systems approaches: Part VII. controllability, stability and parametric designs," *Int. J. Syst. Sci.*, vol. 52, no. 14, pp. 3091–3114, 2021.
[33] J. Huang, H. Fang, L. Dou, and J. Chen, "An overview of distributed high-order multi-agent coordination," *IEEE/CAA J. Automatica Sinica*, vol. 1, no. 1, pp. 1–9, 2014.
[34] C. Hua, K. Li, and X. Guan, "Leader-following output consensus for high-order nonlinear multiagent systems," *IEEE Trans. Autom. Control*, vol. 64, no. 3, pp. 1156–1161, Mar. 2019.
[35] D. W. Zhang and G. P. Liu, "Output feedback predictive control for discrete quasilinear systems with application to spacecraft flying-around," *Asian J. Control*, 2021. [Online]. Available: https://doi.org/10.1002/asjc.2587
[36] K. Ogata, *Discrete-Time Control System*, 2nd ed. Upper Saddle River, NJ, USA: Prentice-Hall, 1995.
[37] Z. Huang, Y. Lu, H. Wen, and D. Jin, "Ground-based experiment of capturing space debris based on artificial potential field," *Acta Astronautica*, vol. 152, pp. 235–241, 2018.
[38] Z. Wei, H. Wen, H. Hu, and D. Jin, "Ground experiment on rendezvous and docking with a spinning target using multistage control strategy," *Aerosp. Sci. Technol.*, vol. 104, 2020, Art. no. 105967.
[39] H. Ousaloo, M. Nodeh, and R. Mehrabian, "Verification of spin magnetic attitude control system using air-bearing-based attitude control simulator," *Acta Astronautica*, vol. 126, pp. 546–553, 2016.
[40] W. Lyu, S. Dai, Y. Dong, Y. Shen, X. Song, and T. Wang, "Attitude motion compensation for imager on fengyun-4 geostationary meteorological satellite," *Acta Astronautica*, vol. 138, pp. 290–294, 2017.
[41] D. L. Chen and G. P. Liu, "A smartphone-based networked control platform: Design and implementation," in *Proc. 39th Chin. Control Conf.*, 2020, pp. 4437–4443.
[42] H. Tan, Z. Huang, and M. Wu, "Development of a customizable real-time monitoring system for networked control systems," in *Proc. 37th Chin. Control Conf.*, 2018, pp. 6350–6355.
[43] Y. G. Xi, *Predictive Control* (in Chinese), 2nd ed. Beijing, China: National Defense Industry Press, 2013.
[44] D. W. Clarke, C. Mohtadi, and P. S. Tuffs, "Generalized prdictive control—Part I. The basic algorithm," *Automatica*, vol. 23, no. 2, pp. 137–148, 1987.
[45] D. W. Zhang and G. P. Liu, "Coordinated control of quasilinear multiagent systems via output feedback predictive control," *ISA Trans.*, 2021. [Online]. Available: https://doi.org/10.1016/j.isatra.2021.10.004

Da-Wei Zhang (Student Member, IEEE) received the B.S. degree in electrical engineering and automation from the China University of Mining and Technology, Xuzhou, China, in 2017 and the M.S. degree in control science and engineering from Northeast Electric Power University, Jilin, China, in 2020. He is currently working toward the Ph.D. degree in control science and engineering with the Department of Control Science and Engineering, Harbin Institute of Technology, Harbin, China.

His research interests include high-order fully actuated systems, predictive control, cooperative control of networked multiagent systems and its applications.

Guo-Ping Liu (Fellow, IEEE) received the B.Eng. and M.Eng. degrees in automation from Central South University, Changsha, China, in 1982 and 1985, respectively, and the Ph.D. degree in control engineering from the University of Manchester, Manchester, U.K., in 1992.

He is currently a Professor with the Southern University of Science and Technology, Shenzhen, China. He has authored/coauthored more than 300 journal papers and ten books on control systems. His research interests include networked multiagent control systems, nonlinear system identification and control, advanced control of industrial systems, and multiobjective optimization and control.

Prof. Liu is a member of Academia Europaea and an IET Fellow.

Lei Cao received the B.S. degree in mechanical engineering from the Nanjing University of Aeronautics and Astronautics, Nanjing, China, in 2014 and the M.S. degree in mechanical engineering from Nanchang University, Nanchang, China, in 2018. He is currently working toward the Ph.D. degree in control science and engineering with the Department of Control Science and Engineering, Harbin Institute of Technology, Harbin, China.

His research interests include networked control systems and Android-based remote laboratories.